Hubble Diagram Dispersion From Large-Scale Structure

Clifton, T; Zuntz, J

Mon. Not. R. Astron. Soc. **000**, 000–000 (0000) Printed 18 June 2013 (MN LATEX style file v2.2)

Hubble Diagram Dispersion From Large-Scale Structure

Timothy Clifton⋆ and Joe Zuntz
Oxford Astrophysics, Physics, DWB, Keble Road, Oxford, OX1 3RH, UK

18 June 2013

ABSTRACT

We consider the effects of large structures in the Universe on the Hubble diagram. This problem is treated non-linearly by considering a Swiss Cheese model of the Universe in which under-dense voids are represented as negatively curved regions of space-time. Exact expressions for luminosity distances and redshifts are used to investigate the non-linear effects of structure on the magnitudes of astrophysical sources. It is found that the intervening voids we consider, between the observer and source, produce changes in apparent magnitude of less than 0.012. Sources inside voids, however, can be affected considerably at redshifts below $z \sim 0.5$. By averaging observable quantities over many randomly generated distributions of voids we find that the presence of these structures has the effect of introducing a dispersion around the mean, which itself can be displaced the background value. Observers in an inhomogeneous universe, who take averages of observables along many different lines of sight, may then introduce systematic biases, and under-estimate errors, if these effects are not taken into account. Estimates of the potential size of these effects are made using data from simulated large-scale structure.

Key words: cosmology: theory – relativity – large scale structure of Universe – supernovae: general – cosmological parameters

1 INTRODUCTION

Hubble diagrams play a key role in our understanding of the evolution of the Universe. It was Hubble diagrams that first led to widespread acknowledgement of the expanding Universe paradigm, and today, in the form of type Ia supernova observations, they provide important evidence for the Dark Energy that is at the heart of the ΛCDM model of the Universe. Ongoing and future projects aim to collect more and more data in order to reconstruct the expansion history of the Universe to ever increasing accuracy, and to test hypotheses about the nature of Dark Energy itself.

Given the extraordinary implications of the supernova results, and the large amounts of resources that are being invested in them, it seems prudent to make sure we fully understand all physical effects that may bias, or influence, the conclusions which are drawn from them. To this end, we perform a detailed, and fully non-linear, investigation of the effects of the simplest large structures on Hubble diagrams.

That structure exists on small scales in the Universe is, of course, indisputable, but while some studies of galaxy surveys have pointed toward homogeneity on scales of $\sim 70h^{-1}$Mpc (Hogg et al. 2005), others have concluded that the largest structures so far detected are limited only by the size of the surveys that found them (Sylos Labini et al. 2008, 2009a,b). The apparent recent detection of an anomalously large local bulk flow (Watkins, Feldman & Hudson 2008), as well as the existence of unexpected features in the CMB (Land & Magueijo 2005; Inoue & Silk 2006), and the CMB dipole itself, also hint at the possibility of large structures existing in the Universe. Here we do not wish to debate the evidence for or against structure existing on different scales, but rather to calculate the effects that different structures have on Hubble diagrams.

The majority of studies in this area have been performed within the context of linear perturbation theory (Dyer & Roeder 1972, 1973, 1974; Sasaki 1987; Futamase & Sasaki 1989; Kasai, Futamase & Takahara 1990; Frieman 1996; Kantowski 1998; Sugiura, Sugiyama & Sasaki 1999; Pyne & Birkinshaw 2004; Bonvin, Durrer & Alice Gasparini 2006; Hui & Greene 2006). Here we treat the problem non-perturbatively by modelling the Universe as a Friedmann-Robertson-Walker (FRW) background, with spherical sections removed and replaced by regions of Lemaitre-Tolman-Bondi (LTB) space-time (Lemaître 1933; Tolman 1934; Bondi 1947). With an appropriate choice of boundary conditions between the FRW and LTB regions, the resulting geometry is an exact solution of Einstein's equations. Such a solution is often referred to as a Swiss Cheese universe, although the replaced regions here are not completely empty. This method should be considered complimentary

⋆ E-mail: tclifton@astro.ox.ac.uk

to studies performed in the linear frame-work: Both require some degree of approximation, but different types of approximation in each case.

The Swiss Cheese approach has a number of drawbacks, but its great benefit is that it allows calculations to be performed beyond the linear level. As the solution is exact, and as it is possible to derive simple expressions for redshift and luminosity distances within it, all higher order and non-perturbative effects are automatically included. Luminosity distances in LTB Swiss Cheese universes have been studied previously by Biswas & Notari (2008); Biswas, Mansouri & Notari (2006); Brouzakis, Tetradis & Tzavara (2007, 2008) and Marra et al. (2007). We will compare our results with these studies as we proceed.

It has been suggested in the literature that non-linear effects from large-scale inhomogeneities may be responsible for the apparent detection of Dark Energy (see, for example, Mattsson (2007)). Our goal here is not to construct a situation in which one can fit for the observations without Dark Energy, but rather to attempt to calculate the effect of inhomogeneities on Hubble diagrams for the purposes of better understanding their influence on parameter estimation, or, conversely, on constraining structure, if cosmological parameters are deemed to be known from elsewhere. Our results indicate that the type of structures expected to exist in the Universe are highly unlikely to be capable of successfully mimicking Dark Energy.

In section 2 we introduce the theory. We will briefly discuss the LTB solution, and how it can be embedded into an FRW universe. We then go on to a more detailed discussion of redshifts and luminosity distances in the resulting space-time. This is done by considering bundles of null geodesics, and the Sachs optical equations.

In section 3 we investigate the effect of a single large void in the Universe on luminosity distances as functions of redshift. Measures of distance to objects on the other side of the void appear largely unaffected by its presence, with changes in apparent magnitude of less than 0.012, for the voids we consider. This is consistent with linear treatments, such as that of Frieman (1996), as well as previous non-linear treatments, such as that of Brouzakis, Tetradis & Tzavara (2007, 2008). Observations of objects that reside inside the void, however, can be considerably affected by the void's presence, with shifts in apparent magnitude of up to 0.2 being easily obtainable at low redshifts ($z < 0.2$). At higher redshifts the effect on objects inside the void drops off, and becomes sub-dominant compared to the small effect of looking through them. We present results for the change in luminosity distance that can result from voids of varying depths, widths and at different redshifts. Results here are limited to the case of looking through the centre of voids.

Section 4 contains an analysis of the effect of looking through many voids in a row. In this section the voids are drawn from idealised distributions. Examples are presented, and the case of averaging over many lines of sight is analysed. Such averaging of luminosity distances, for specified geometries, appears to us to be a preferable, if more cumbersome method, than averaging the mass distribution, and calculating a single luminosity distance in the corresponding geometry. We present results for the dispersion, and deviation, of Hubble diagrams that results from different distributions of voids. As the considerations of single voids suggests, the effect of objects located inside voids contributes most of the dispersion at low redshifts, while at high redshifts the dispersion is mainly due to the cumulative effect of looking through voids.

In section 5 we make an attempt at linking the idealised cosmologies, considered in previous sections, to some more realistic distributions of matter. The idea here is that instead of taking purely idealised distributions of voids, we take density profiles from simulated large-scale structure, and then use these distributions to motivate our Swiss Cheese models. To achieve this we consider simulated structure generated from the Millennium Simulation. These profiles are produced by a process of averaging over different length scales. The profiles obtained are then idealised, so as to fit into the framework developed in the preceding sections, and the results on Hubble diagrams are calculated. This method is not proposed as a way of superseding the linear treatment of distance measures within these space-times (which would manifestly be applicable here, as they are created in the linear regime). Rather, we intend it to be a method of obtaining realistic distributions of voids from a well motivated source.

Finally, in section 6, we conclude. The Appendix shows an interesting example of another case that can be solved for exactly.

2 SWISS CHEESE COSMOLOGY

The cosmology we consider here is an FRW background with spherical regions removed and replaced with LTB space-times, in order to model inhomogeneities. Sub-sections 2.1-2.3 recap results on LTB space-times, boundary conditions for embedding LTB patches into FRW, and expressions for null geodesics and redshifts in LTB. Sub-section 2.4 then contains a discussion of luminosity distances in these space-times, for both observer and source away from the centre of symmetry. The FRW and observer centred limits of these expressions are found in sub-section 2.5.

2.1 The LTB Solution

The LTB line-element is given by (Lemaître 1933; Tolman 1934; Bondi 1947)

$$ds^2 = -dt^2 + \frac{R'^2}{(1-kr^2)}dr^2 + R^2 d\Omega^2, \tag{1}$$

where $R = R(t,r)$, $k = k(r)$ and prime denotes partial differentiation with respect to r. For $\Lambda = 0$ and $k < 0$ we can write R in parametric form as

$$R = \frac{m(1-\cosh\Theta)}{2kr^2} \tag{2}$$

$$t - t_0 = \frac{m(\sinh 2\Theta - 2\Theta)}{2(-kr^2)^{3/2}} \tag{3}$$

where $t_0 = t_0(r)$ and $m = m(r)$. Exact solutions exist for $\Lambda \neq 0$, and are given in terms of elliptic functions by Zecca (1991). It is also possible to solve for the case with $k \geqslant 0$, but this will not be required here. The geometry (1) is an exact solution of Einstein's equations in the presence of a perfect fluid of pressureless dust with energy density

$$\rho = \frac{m'}{R^2 R'}. \tag{4}$$

Gauge freedoms allow us to transform into a coordinate system in which $t_0 =$ constant, without loss of generality. The LTB space-time is then completely specified by a choice of $k(r)$ and $m(r)$, and reduces to FRW in the limit $k(r)$ and $m(r)$ =constant. We will refer to $k(r)$ as the spatial curvature and $m(r)$ as the gravitational mass distribution.

2.2 Boundary Conditions

We now wish to replace regions of FRW with the LTB geometry described above. To do this we need the conditions required to match a manifold with metric (1) to one with FRW metric

$$ds^2 = -dt^2 + a^2(t)\left(dx^2 + f^2(x)d\Omega^2\right) \tag{5}$$

at a boundary of constant $r = x = \Sigma$. The Darmois junction conditions imply that the matching is a solution of Einstein's equations if the first and second fundamental form on the hyper-surface at Σ are identical on either side (Bonnor & Vickers 1981). This corresponds to the two conditions (Ribeiro 1992)

$$R|_\Sigma = af|_\Sigma \tag{6}$$

$$\sqrt{1-kr^2}|_\Sigma = f'|_\Sigma. \tag{7}$$

It can be shown that equations (6) and (7) imply that the 'Bondi mass' inside the excised region should equal the mass of the FRW region that was removed (Ribeiro 1992):

$$\begin{aligned} m^{(LTB)} &= 4\pi \int \rho R' R^2 dr \\ &= 4\pi \int \rho a^3 f^2 f' dx = 4\pi \rho a^3 f^3 = m^{(FRW)}, \end{aligned} \tag{8}$$

where $m^{(LTB)}$ in the mass from Eq. (4). These conditions can be verified to describe the requirement that the LTB metric should reduce to FRW at the boundary.

2.3 Null Geodesics and Redshifts

Now consider a null geodesic in (1) with affine parameter λ, and with a tangent vector $k^a = dx^a/d\lambda$. If n^a is the unit vector in the direction of k^a, in the rest space of an observer with 4-velocity u^a, then k^a can be decomposed as

$$k^a = (-u_b k^b)(u^a + n^a), \tag{9}$$

where $u_a u^a = -1$, $n_a n^a = 1$ and $u_a n^a = 0$. Thus, for a radial null geodesic, and an observer co-moving with the coordinate system (1), we have $u^a = (1,0,0,0)$ and $n^a = (0, \pm\sqrt{1-kr^2}/R', 0, 0)$. The $\pm$ sign here corresponds to geodesics directed away, or toward, the centre of symmetry, and we have chosen λ to increase with t. According to (9), an infinitesimal increment in affine parameter, $d\lambda$, will then be seen by the observer following u^a as changes in time and position of

$$dt = -u_a k^a d\lambda \tag{10}$$

$$dr = \mp u_a k^a \frac{\sqrt{1-kr^2}}{R'} d\lambda. \tag{11}$$

This agrees with the equation for radial null geodesics, which can be read off from (1) as

$$\frac{dr}{dt} = \pm \frac{\sqrt{1-kr^2}}{R'}. \tag{12}$$

The tangent vectors for radial geodesics can now be written as $k^a = (A, B, 0, 0)$, where $A = A(t,r)$ and $B = B(t,r)$. The trajectories to which k^a are tangent are both null and geodesic, so that $k^a k_a = 0$ and $k^a k^b{}_{;a} = 0$. This gives $B = \pm A\sqrt{1-kr^2}/R'$, and

$$k^a = A\left(1, \pm\frac{\sqrt{1-kr^2}}{R'}, 0, 0\right), \tag{13}$$

where A as the solution of

$$\pm\sqrt{1-kr^2}A' + \dot{A}R' + A\dot{R}' = \frac{dA}{dt}R' + A\dot{R}' = 0. \tag{14}$$

This expression integrates to

$$A \propto \exp\left\{-\int \frac{\dot{R}'}{R'} dt\right\}. \tag{15}$$

As always, the redshift of a photon is given by

$$1 + z = \frac{(u^a k_a)_e}{(u^b k_b)_o}, \tag{16}$$

where subscript e denotes a quantity at the point where the photon is emitted, and subscript o a quantity at the point it is observed. In the present situation we have $u^a k_a = -A$, so the redshift is

$$1 + z = \frac{A_e}{A_o} = \exp\left\{\int_e^o \frac{\dot{R}'}{R'} dt\right\}, \tag{17}$$

in agreement with the source centred case considered by Bondi (1947), and the observer centric case considered by Ribeiro (1992). This expression is valid for any source and observer connected by a radial geodesic, if they are centred or not.

2.4 Luminosity Distances

Consider a bundle of null geodesics with cross-sectional area $d\sigma$, and tangent vector k^a. The rate of change of $d\sigma$ along the bundle is

$$\frac{d(d\sigma)}{d\lambda} = k^a{}_{;a} d\sigma, \tag{18}$$

and is independent of the 4-velocity of the screen onto which it is projected (Sachs 1961). Differentiating this expression with respect to λ gives the second order Sachs optical equation:

$$\frac{1}{\sqrt{d\sigma}} \frac{d^2\sqrt{d\sigma}}{d\lambda^2} = -\left(|\varsigma|^2 + \omega^2 + \frac{1}{2}R_{ab}k^a k^b\right), \tag{19}$$

where $|\varsigma|^2 = k_{(a;b)}k^{a;b}/2 - (k^a{}_{;a})^2/4$ is the shear, and $\omega^2 = k_{[a;b]}k^{a;b}/2$ is the rotation of the bundle. For radial geodesics we then have $\varsigma = 0$, from symmetry considerations, and we can set $\omega = 0$, as the sources under consideration are effectively point-like.

For the radial geodesics (13), in the space-time (1), the right hand side of equation (19) can be shown to be given by (Biswas, Mansouri & Notari 2006)

$$\frac{1}{\sqrt{d\sigma}} \frac{d^2\sqrt{d\sigma}}{d\lambda^2} = \frac{1}{R}\frac{d^2 R}{d\lambda^2}, \tag{20}$$

which can be verified using (10), (11) and (14). The solution to this equation is given by

$$\sqrt{d\sigma} \propto R \int \frac{d\lambda}{R^2}, \tag{21}$$

where the constant of proportionality can be found by considering the limit $d\sigma \to 0$, when the beam is focused at the observer. We then have

$$\frac{d\sqrt{d\sigma}}{d\lambda} \to d\Omega, \tag{22}$$

where $d\Omega$ is the square root of the solid angle subtended by the beam. Enforcing this limit in equation (21) gives

$$\sqrt{d\sigma} = d\Omega R_o R \int \frac{d\lambda}{R^2}, \tag{23}$$

where R_o is the value of R at the observer, where the beam is focused.

The angular diameter distance along a radial geodesic in this space-time is then given by

$$r_A \equiv \frac{\sqrt{d\sigma_e}}{d\Omega} = R_o R_e \int_o^e \frac{d\lambda}{R^2}, \tag{24}$$

which is the expression obtained by Biswas, Mansouri & Notari (2006). The galactic angular distance, along the same geodesic, is then given by Etherington's theorem (Etherington 1933) as

$$r_G = (1+z) R_o R_e \int_o^e \frac{d\lambda}{R^2}, \tag{25}$$

and the luminosity distance is

$$r_L = (1+z)^2 R_o R_e \int_o^e \frac{d\lambda}{R^2}. \tag{26}$$

This is the required expression for luminosity distance, applicable when both source and observer are off centre.

2.5 FRW and Observer-Centric Limits

To clarify how the redshifts and distance measures described above relate to more usual expressions we will now consider the FRW, and observer centred LTB limits of these equations.

In the FRW limit of LTB space-times we have that $k(r)$ and $m(r) \to$constant and, consequently, $R(t,r) \to a(t)r$. In this limit the LTB line-element (1) reduces to its FRW counterpart. It can also be seen that the expression for redshift, equation (17), reduces to

$$1 + z \to \exp\left\{ \int_e^o \frac{\dot{a}}{a} dt \right\} = \frac{a_o}{a_e}, \tag{27}$$

which is, of course, the usual FRW expression.

If we now consider the angular diameter distance, (24), we can see that, using (11) and (14), this reduces to

$$r_A \to a_0 a_e r_o r_e \int_o^e \frac{dr}{r^2\sqrt{1-kr^2}} = a_o a_e r_o r_e \left[\frac{\sqrt{1-kr^2}}{r} \right]_e^o, \tag{28}$$

as, in this limit, we have $A \propto 1/a$. To confirm that this is the usual FRW angular diameter distance it is convenient to transform to the proper radial coordinate, l, via $r = f(l)$, where:

$$\begin{array}{lll} f(x) = \sin(x) & & k = 1 \\ f(x) = x & \text{for} & k = 0 \\ f(x) = \sinh(x) & & k = -1. \end{array} \tag{29}$$

The FRW limit of the angular diameter distance can then be written in the more familiar form

$$r_A \to \frac{f(\Delta l)}{(1+z)}, \tag{30}$$

where $\Delta l = |l_e - l_o|$. The Minkowski limit follows from this, with $a =$constant and $k = 0$, and is given by $r_A \to \Delta r$.

Finally, let us consider the observer centric case, which should follow from the more general expressions above when $R_o \to 0$. The most convenient way to find this limit is to differentiate (24), with respect to λ, to obtain

$$\frac{1}{R_e}\frac{dr_A}{d\lambda} - \frac{r_A}{R_e^2}\frac{dR_e}{d\lambda} = \frac{R_o}{R_e^2} \to 0. \tag{31}$$

Integrating the left-hand side of this then gives

$$r_A \propto R_e, \tag{32}$$

which is the expected form of the angular diameter distance for an observer at the centre of symmetry (Bondi 1947). The expression for redshift, (17), can immediately be seen to reduce to the observer centred case considered by Ribeiro (1992), as $r_o \to 0$.

The expressions for redshift and luminosity distance, (17) and (26), therefore have the correct FRW, Minkowski and observer centred limits, and reduce to the known expressions as they are approached.

3 A SINGLE VOID

We will now consider the case of a flat FRW Universe containing a single void. We can choose coordinates, without loss of generality, such that $t_0 =$constant, and so that the big bang occurs simultaneously at all points in space. This condition is automatically satisfied in FRW if surfaces of constant density are chosen to be surfaces of equal time. We also choose initial conditions such that $m \propto r^3$, so that the gravitational mass is initially evenly distributed. The form of the void is then specified by the function $k(r)$, which we will take to be a smooth curve of the form

$$k = \frac{k_0}{2}\left[1 + \cos\left(\pi \frac{r}{r_0}\right)\right], \tag{33}$$

where $k_0 < 0$ and $r_0 > 0$ are constants specifying the depth and width of the void, respectively. This negative perturbation in k is a smoothly varying function of r, that reduces to 0 at the edge of the void, $r = r_0$. The negative curvature causes the space inside the void to expand faster than that outside, so that the energy density inside the void is dissipated more rapidly. An under-density then occurs, not due to any any decrease in gravitational mass, but due to an increase in spatial volume. Although the choices above appear reasonably natural, one may consider more general space-times, either by changing the functional form of $m(r)$ and $k(r)$, or by considering less symmetric space-times than that of LTB. We will postpone considering the effects of such generalisations here, so that we can first concentrate on the simple case of the smooth perturbation in curvature outlined above.

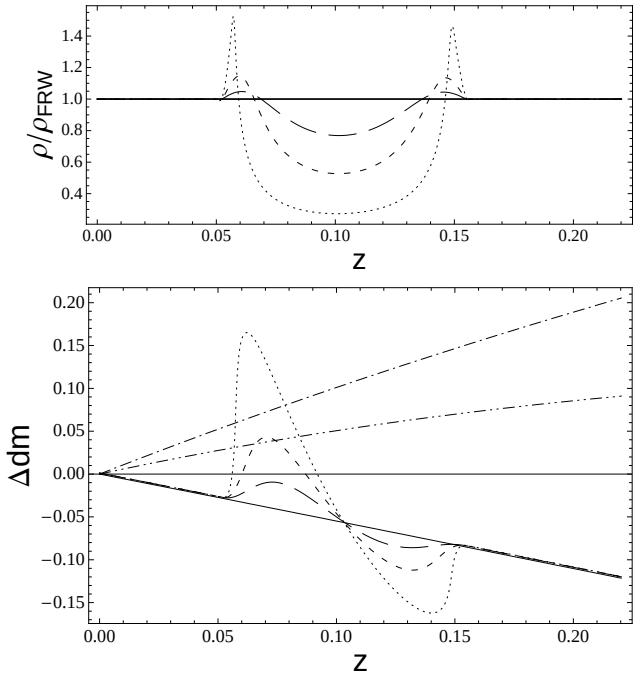

Figure 1. The upper panel shows the fractional energy density experienced by the photon, where the long-dashed, short-dashed and dotted lines correspond to voids that are 25%, 50% and 75% under-dense today. The lower panel show how these three voids effect the distance modulus. The solid, dot-dashed and double-dot-dashed lines in this plot correspond to EdS, dS and ΛCDM with $\Omega_\Lambda = 0.7$, respectively. These results are with an EdS background.

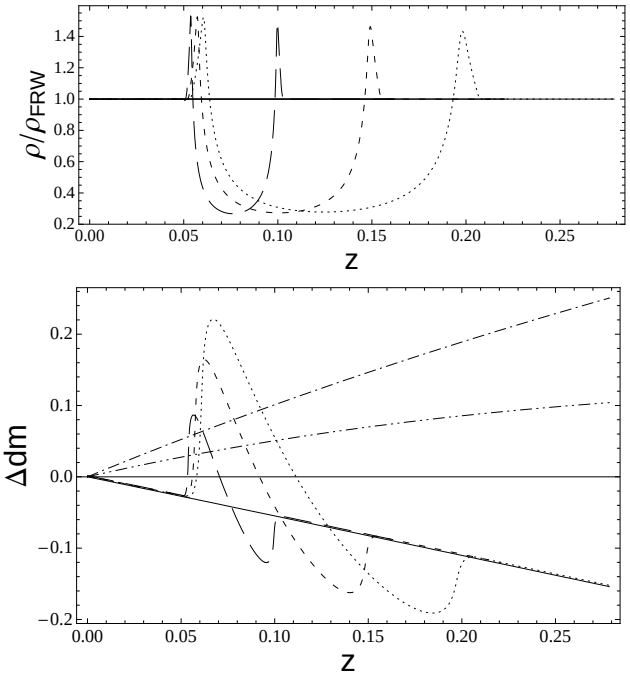

Figure 2. The upper panel shows the fractional energy density for three voids of the same depth, but with varying widths. The lower panel shows the corresponding effect on the distance modulus. Dot-dashed, double-dot-dashed and solid lines are as in Figure 1. These results are with an EdS background.

3.1 An Einstein-de Sitter background

Consider the case of a void in a space-time that is asymptotically a spatially flat Einstein-de Sitter (EdS) universe, as $r \to r_0$ in (1). In this case $\Lambda = 0$, and the metric functional $R(t, r)$ is given parametrically by equations (2) and (3). The functions $t = t(z)$ and $r = r(z)$, along past null geodesics, can then be found by integrating equations (12) and (17). Substituting these expressions into equation (26) gives $r_L(z)$. Here we will use this result to investigate the effects such structures have on Hubble diagrams, when observers look through them.

We begin by considering the effect of voids with varying width and depth, at the same position. For ease of computation we consider the space-time as an LTB under-density matched to an FRW background under the conditions (6) and (7), at $r = r_0$. The geodesic equations, and redshift relations, must now be integrated in each space-time and $r(z)$ and $t(z)$ matched at the boundaries. The cumulative redshift, $1 + z_T$, is given in the usual way by the expression

$$(1 + z_T) = \prod_i (1 + z_i),$$

where $1+z_i$ is the redshift along a portion, i, of the geodesic.

The effects of three voids with different depths, all approximately the same width and located at the same redshift ($z \sim 0.1$) are shown in Figure 1. The upper plot shows the energy density encountered by a photon as it travels through the three different voids, and the lower plot shows the corresponding distance modulus, Δdm, as a function of redshift, z. Distance modulus is defined as the magnitude an object appears at, minus the magnitude it would have at the same redshift in a empty, negatively curved Milne universe. It can be written in terms of luminosity distance as

$$\Delta\text{dm} = 5 \log_{10} r_L - 5 \log_{10} r_L^m, \tag{34}$$

where r_L is given by (26), and $r_L^m = z + z^2/2$ is the expansion normalised luminosity distance in a Milne universe. Anything below Δdm=0 in Figure 1 is then interpreted as a decelerating universe, and anything above it as accelerating. For reference, we have included in this plot the distance moduli for an EdS universe, as the solid line, and for a de Sitter (dS) space, as the dot-dashed line. A ΛCDM cosmology, with $\Omega_\Lambda = 0.7$, is shown as the double-dot-dashed line.

It can be seen from the upper plot of Figure 1 that, although the spatial curvature k is always negative, the energy density can reach values in excess of the asymptotic value at the edge of the void. This is due to the analogue of the radial scale factor, R', being lower than its asymptotic value in this region. Aside from these small over-densities, at the edges of the void, it can clearly be seen that the energy density in the centre of the void has been dissipated as a result of the more rapid expansion there, caused by the negative curvature perturbation. The three voids shown in this plot are chosen such that at the their centres they are 25%, 50% and 75% under-dense at the present time. The upper plot shows these regions to be slightly less under-dense than this at their minima, as what is depicted is the energy density experienced by the photon as it passed through them, sometime before the present.

The lower plot in Figure 1 shows that there is no noticeable effect, due to the void, on viewing objects that are

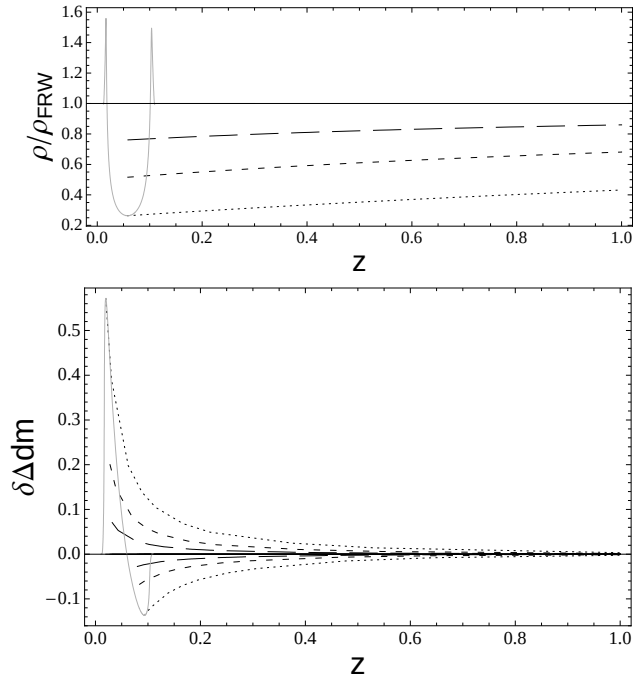

Figure 3. The effect of changing the location of the void. The three voids from Figure 1 are moved to different redshift between $z = 0.1$ and 1. The upper panel shows how the fractional energy density at the centre of the voids varies with redshift. The lower panel shows the maximum displacement in distance modulus, from the background value, that these voids cause. These results are with an EdS background.

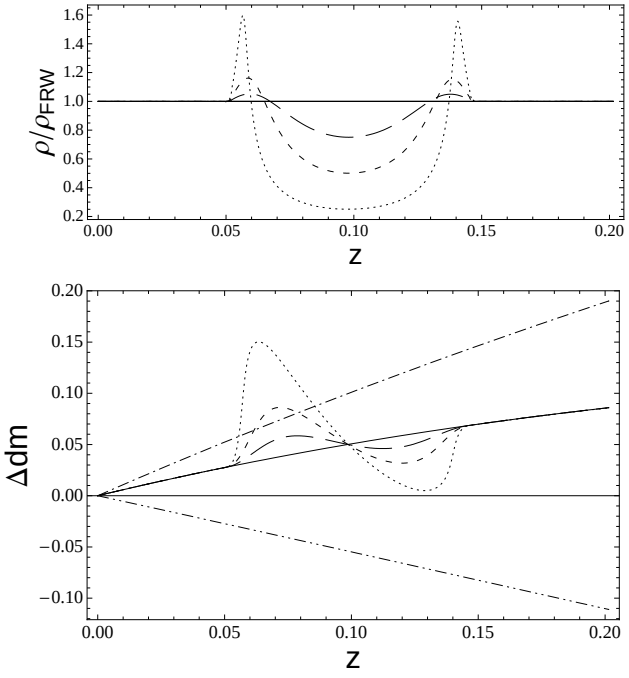

Figure 4. The upper panel is the same as in Figure 1, but the background is now ΛCDM with $\Omega_\Lambda = 0.7$. The lower panel shows the corresponding distance moduli. The solid line in this plot again shows the background, which is now ΛCDM, and the double-dot-dashed line shows EdS.

beyond it. While the presence of the voids causes a deviation from the EdS background in their vicinity, it can be seen their distance moduli return to within 0.01 of the background value at redshifts beyond. Weak lensing effects are expected to be within this order of magnitude (see e.g. Frieman (1996)) as well as the late-time integrated Sachs-Wolfe effect (see e.g. Granett, Neyrinck & Szapudi (2008)). However, it seems unlikely that such small effects will be detectable in Hubble diagrams that are constructed from supernovae observations, at least in the foreseeable future[1]. Hence, the principle effect of these structures appears to be on objects that are inside the voids themselves, in which case the deviation from the background value can be seen to be considerable for the examples shown here. Clearly these deviations are a function of the void depth, and increase in a proportionate way. We note this effect is appears to be largely due to the $0.1 - 0.3$ perturbations that appear in the metric functional $R(t, r)$. Such large metric perturbations are unlikely to develop in the linear approach, and so this effect may not show up in such a pronounced way in treatments of that kind.

The small effect of the voids on viewing objects behind them is in accordance with the studies of Brouzakis, Tetradis & Tzavara (2007, 2008) and Biswas & Notari (2008), who found similar results in their studies of luminosity distances in Swiss cheese. The maximum shift in apparent magnitude for objects also seems consistent with the results of Biswas & Notari (2008), who find the effect of a void with a 50% under-density at its centre produces a change in apparent magnitude of $\delta\Delta\text{dm}\sim 0.4$. This can be seen to be similar to that found in Figure 1.

As well as varying the depth of a void, we will also be interested in the effect of varying its width, and its distance from us. This is shown in Figures 2 and 3. In Figure 2 all three example voids are now chosen to have the same depth, so that they are 75% under-dense today, while their width is varied. The deviation from the background distance modulus changes its width accordingly, and as would be expected. We note that the maximum deviation is larger for the widest voids, decreasing substantially as the width of the void is decreased.

In Figure 3 we show the effect of considering voids at different distances from us. We consider three sets of voids, one set that is 25% under-dense today, another that is 50% under-dense, and a third that is 75% under-dense. The upper plot in this figure shows how the maximum depth of void varies with redshift, for each set of voids. As expected, as the centre of the void is moved to greater redshifts, the minimum density experienced by the photon increases. This is due to the depth of voids increasing with time. All the voids considered here are 0.1 redshifts wide today. We do not consider voids that are centred at $z < 0.1$, as we are interested in the effect of distant voids, and not the effect of us living in a void, which is considerable in itself (Alexander, Biswas & Notari 2007; Alnes, Amarzguioui & Grøn 2006; Garcia-Bellido & Haugboelle 2008; Clifton, Ferreira & Land 2008; Bolejko & Wyithe 2008). In the lower plot of Figure 3 we show the maximum deviation

[1] The 'intrinsic errors' in the magnitude of supernovae are currently of the order $0.1 - 0.2$.

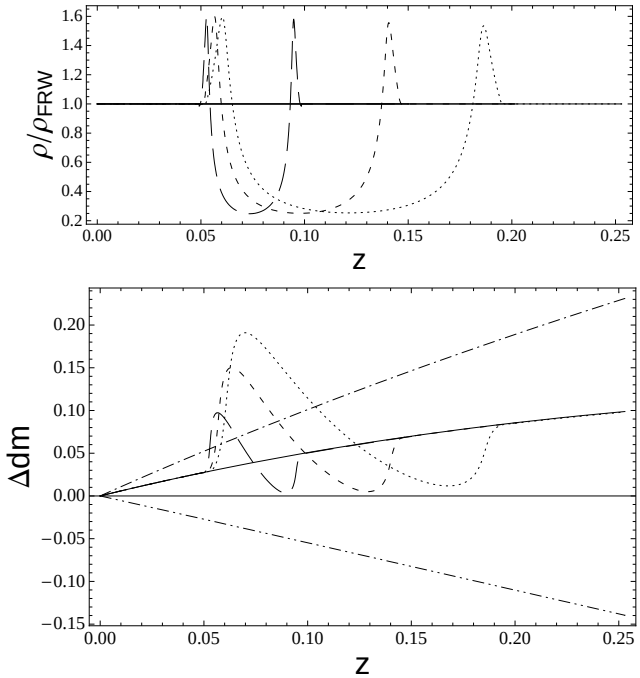

Figure 5. The upper panel is the same as Figure 2, but now with a ΛCDM background with $\Omega_\Lambda = 0.7$. The lower panel shows the corresponding distance moduli, with the solid and double-dot-dashed lines as in Figure 4.

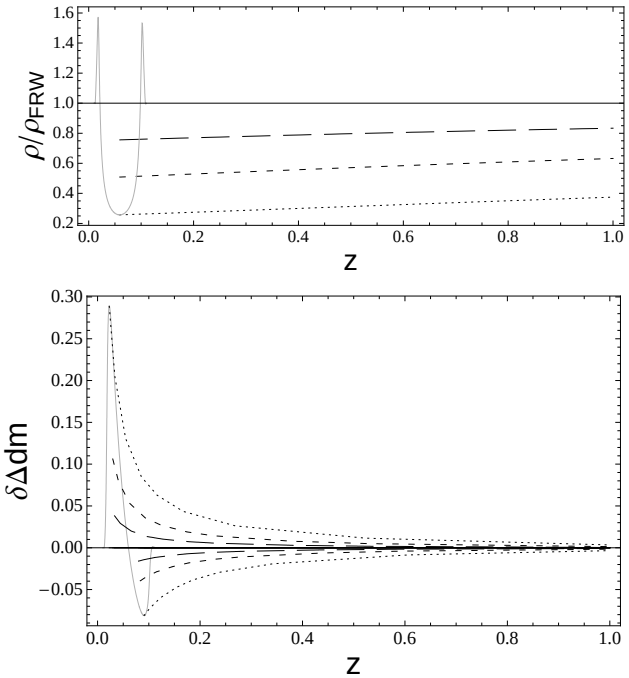

Figure 6. The same as Figure 3, but with a ΛCDM background with $\Omega_\Lambda = 0.7$.

in distance modulus, from the background value, for each of the three sets of voids. This maximum deviation can again be seen to be proportionate to the maximum depth of void, as experienced by the photon, and shown in the upper plot. It can be seen that the maximum deviation in distance modulus is highly sensitive to the location of the void, and increases steeply at low z.

3.2 A ΛCDM background

As well as a spatially flat, dust dominated EdS background, we are also interested in backgrounds containing a non-zero Λ. To achieve an understanding of this we will repeat the analysis above for the case of a single void in an asymptotically ΛCDM universe with $\Omega_\Lambda = 0.7$ [2]. In this case the equations for $r(t)$, $z(t)$ and r_L are unchanged, with the functional form of $R(t, r)$ modified from that given in (2) and (3), in order to include the effects of Λ (Zecca 1991).

Figure 4 shows the same three voids as Figure 1, with under-densities of 25%, 50% and 75% and centred at $z \sim 0.1$. The background is again given by a solid line, but this now corresponds to ΛCDM with $\Omega_\Lambda = 0.7$. The EdS distance modulus is shown by the double-dot-dashed line. The effect of the void can be seen to be similar that shown in Figure 1, when $\Lambda = 0$, but with a smaller magnitude. The distance modulus returns to within 0.01 magnitudes of the background at large z, and there is a considerable, though smaller, displacement from the background value when looking at objects inside the void. It can be seen that the energy density experienced by the photon is closer to the value of the under-density today in this case, reflecting the fact that the growth of structure slows when Λ comes to dominate.

Figure 5 illustrates the dependence of the distance modulus on the width of void in this background, and the results can be seen to be very similar to those deduced from Figure 2, but again with a smaller overall magnitude of the displacement. The maximum deviation from the background is again sensitive to the depth of the void, as well as its width. In Figure 6 we consider the maximum deviation of the distance modulus from its background value, for the same three sets of voids as in Figure 3. The results are similar to the EdS case, the principle differences appearing to be the smaller magnitude of the displacement, and the weaker dependence of the depth of under-density on z, due to the suppression of structure formation in the presence of Λ. This manifests itself in the upper plot of Figure 6 as a slightly shallower gradient.

3.3 Lensing

The previous subsections have shown that at low redshift, in both EdS and ΛCDM backgrounds, the principal effect of large voids is on objects that are viewed within them. In this case the displacement of the distance modulus due to intervening voids is a smaller, sub-dominant, effect. At higher redshifts, however, the effect of voids on objects within them is much smaller. In this case the lensing effect, due to looking through voids, becomes relatively more important. In this subsection we quantify the size of this effect for different sized voids, with different widths, at different redshifts, in both EdS and ΛCDM backgrounds.

First let us consider an EdS background. In Figure 7 we plot the displacement from the distance modulus of the EdS background due to a single void. We consider three depths

[2] With radiation neglected, which should a good approximation in the epochs under consideration.

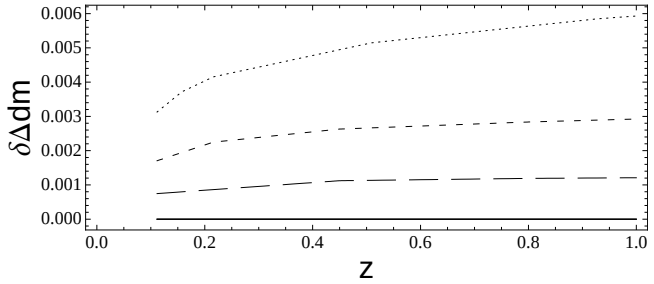

Figure 7. The displacement from the background distance modulus when looking through a single void, at different distances, in an EdS background. The long-dashed line corresponds to voids with a central under-density of 25% today, the short-dashed line to 50% today, and the dotted line to 75%. The energy density experienced by the photon is given by the upper plot in Figure 3. The values of $\delta\Delta$dm are plotted at the redshift that the photon leaves the void. All voids here have a width of $\Delta z = 0.1$.

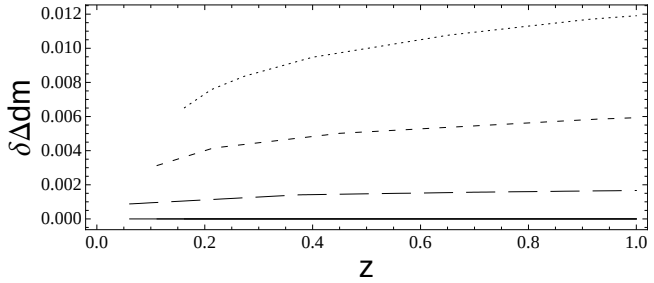

Figure 8. The same as in Figure 7, but the voids considered are now all 75% under-dense at their centre today. The long-dashed, short-dashed and dotted lines now correspond to voids with widths of $\Delta z = 0.05$, 0.10 and 0.15. These results are with as EdS background.

of void in this plot, with central under-densities today of 25%, 50% ad 75%. All the voids currently under consideration have a width, measured by an observer standing at their edge today, of $\Delta z = 0.1$. The density profile experienced by a photon for these three void depths, as they are moved to different distances from the observer, are the same as is shown in the upper plot of Figure 3. What is plotted here is the displacement from the background distance modulus at the moment the photon leaves the void. It is clear from Figure 7 that the lensing effect, while smaller than the effects on the distance modulus shown in Figure 3, is considerably less sensitive to the distance of the void, and, in fact, increases somewhat as the void is moved further away. Increasing the depth of the void increases the magnitude of this effect, in a similar way to was shown in Figure 3.

Figure 8 shows the effect of looking through a single void, at different distances, in an EdS background, but now varying the width of the void, instead of its depth. All voids are now 75% under-dense at their centre today, but now have widths of $\Delta z = 0.05$, 0.10 and 0.15, depicted as the long-dashed, short-dashed and dotted lines, respectively. Again, $\delta\Delta$dm is given in this plot at the moment the photon leave the void. It can be seen that the lensing affect is sensitive to the void width, and increases with the width of the void.

Now let us consider a ΛCDM background, with $\Omega_\Lambda = 0.7$. The results of considering voids with different depths, at different distances, are shown in Figure 9. The results are similar to the EdS case, but the magnitude of the affect

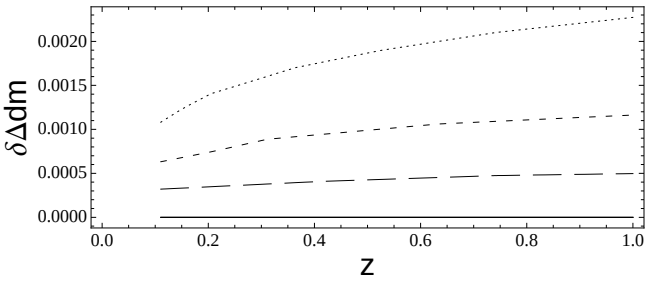

Figure 9. The same as Figure 7, but in a ΛCDM background, with $\Omega_\Lambda = 0.7$. The long-dashed, short-dashed and dotted lines correspond to voids with 25%, 50% and 75% under-densities.

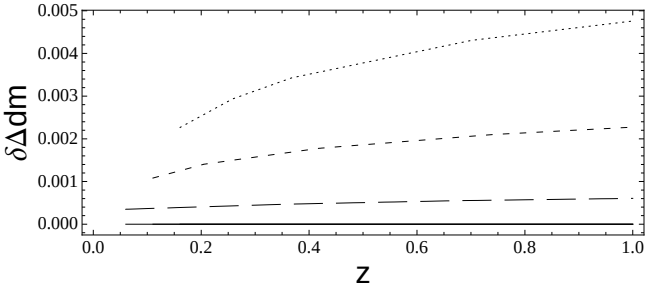

Figure 10. The same as Figure 8, but in a ΛCDM background, with $\Omega_\Lambda = 0.7$. The long-dashed, short-dashed and dotted lines correspond to voids with widths of $\Delta z = 0.05$, 0.10 and 0.15.

is smaller, in keeping with the results found for looking at objects inside the voids. In Figure 10 we consider voids with different widths, and the same depth, at different distances. Again, the results are comparable to those found in an EdS background, but with a smaller magnitude.

4 MANY VOIDS

The effect of a single void on Hubble diagrams is of some interest by itself. Such effects could be used to search for hypothesised large structures, such as that which is supposed to explain the CMB cold spot (Inoue & Silk 2006). However, if we suppose that a single large void exists in the Universe, then it is natural to think that there will be other structure on similar scales. In this section we consider just such a scenario, with many LTB voids lined up back to back in an FRW background.

4.1 An Einstein-de Sitter background

Again, we will first consider the case of a spatially flat EdS background. Now instead of inserting a single void, satisfying the boundary conditions (6) and (7), we will insert a number of voids. As before, we will match these voids to the background cosmology at $r = r_0$, where they are locally FRW. The choice of voids that can be used for this process is quite arbitrary. Here we will randomly select voids from a couple of different distributions, in order to gain some understanding. This process can, of course, be repeated for any distribution of voids one may wish to consider.

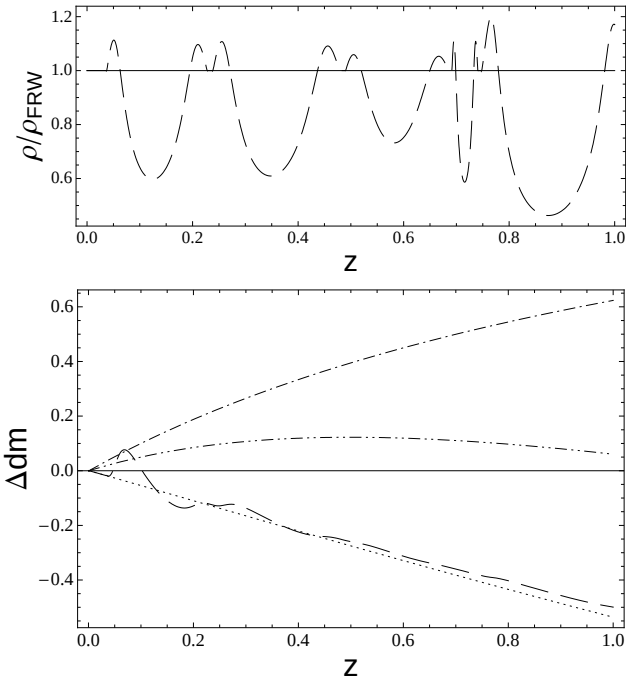

Figure 11. The upper panel shows a sample set of voids taken from the deep distribution of voids, A. The lower plot shows the corresponding distance modulus. The dot-dashed and double-dot-dashed lines are as in Figure 1. The dotted line is EdS. These results are with an EdS background.

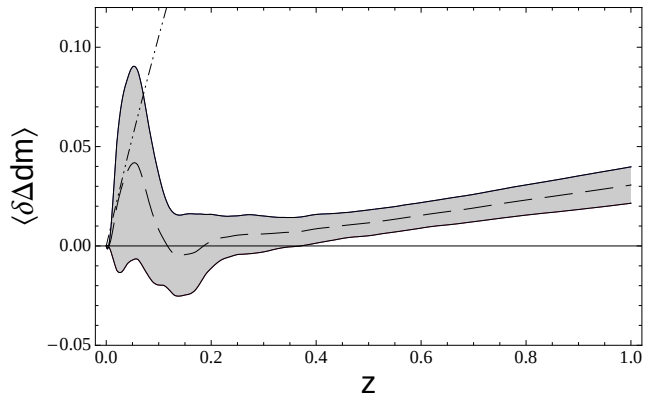

Figure 12. The result of averaging the distance moduli of 1000 sets of voids randomly drawn from the deep distribution, A. Displayed is the mean deviation from the EdS background, the dashed line, and the standard deviation about that mean, the grey area. Also displayed for reference is the deviation of ΛCDM with $\Omega_\Lambda = 0.7$ from EdS, as the double-dot-dashed line.

4.1.1 Distribution A: Deep voids

For this example we will consider voids with present day depths drawn from a flat distribution between 0% under-dense and 75% under-dense today. The width of voids will be drawn from a flat probability distribution, and will be between 0.01 and 0.19 redshifts wide when viewed by an observer standing at their edge today. Although these choices allow for the existence of large structures, we do not consider them extreme (i.e. they are only a fraction under-dense, not completely empty).

In Figure 11 we show an example set of voids, out to

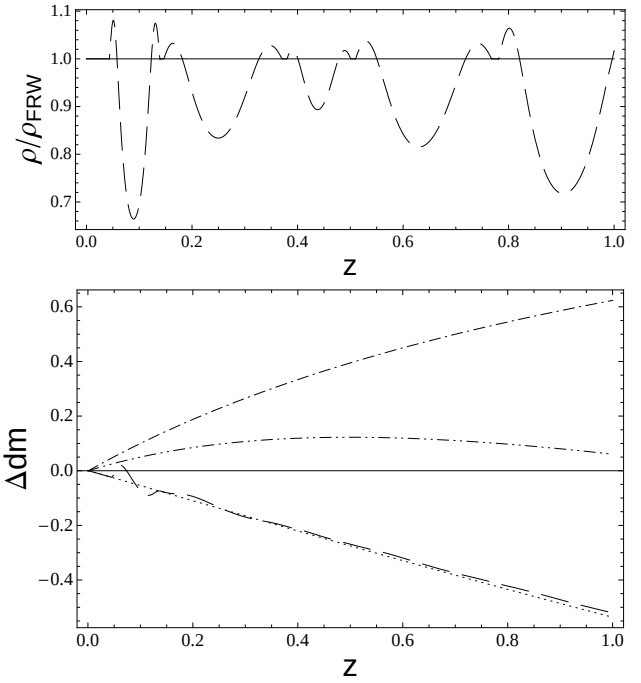

Figure 13. The same as Figure 11, but with voids drawn from the shallow distribution, B.

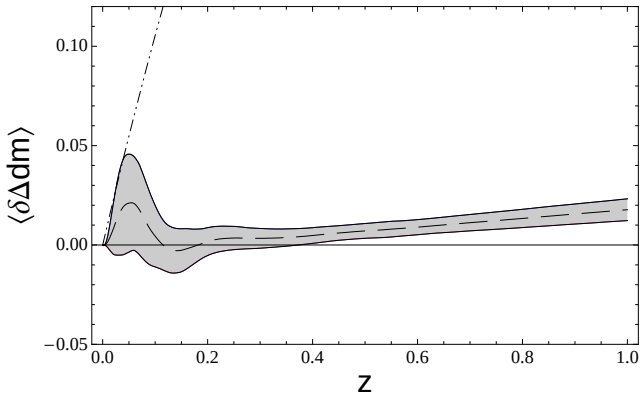

Figure 14. The same as Figure 12, but with voids drawn from the shallow distribution, B.

$z = 1$, picked from this distribution. As was the case previously, the upper plot shows the energy density encountered by a photon that reaches us at the present day. We ensure that we are not in a void by placing the edge of the first void at a redshift of $z = 0.01 + w$, where w is a random number between 0 and 0.05 (the reason for introducing w will be made clear shortly). The dotted line in the lower plot is the background FRW universe, which here is EdS. The dot-dashed lines and double-dot-dashed lines represent the distance moduli of dS and ΛCDM with$\Omega_\Lambda = 0.7$, respectively. While there are clear deviations from the background distance modulus, it seems highly unlikely that a distribution of voids of this type could be mistaken for ΛCDM with $\Omega_\Lambda = 0.7$.

Having considered an example set of voids, it is now of interest to consider the average of many different sets drawn from the same probability distribution. This may be the type of process that one would wish to consider when col-

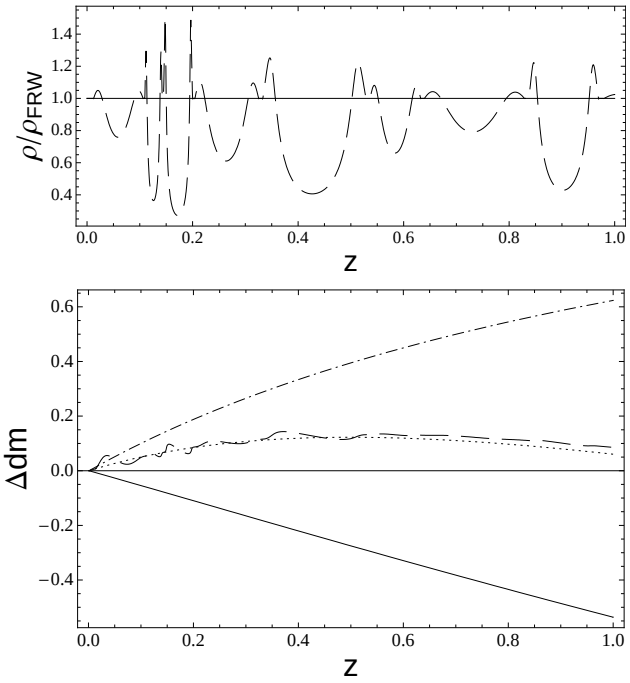

Figure 15. The same as Figure 11, but with a ΛCDM background with $\Omega_\Lambda = 0.7$. This set of voids is from distribution A.

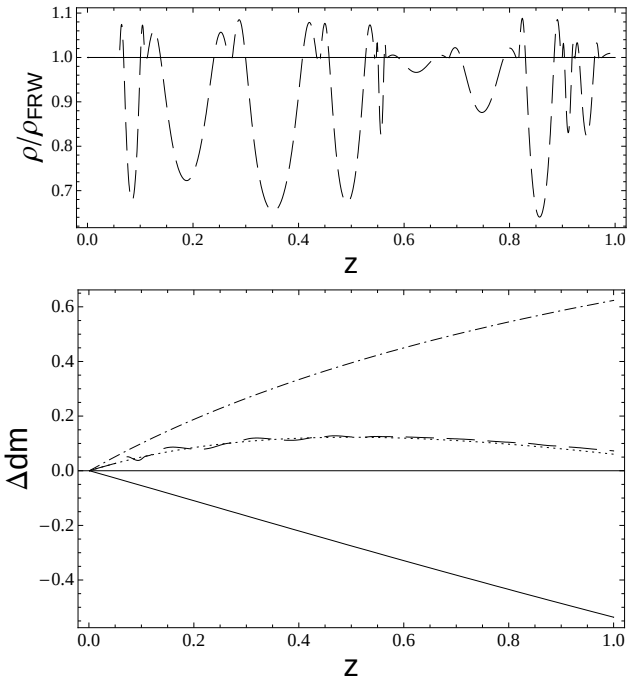

Figure 17. The same as Figure 15, but with the shallow void distribution, B.

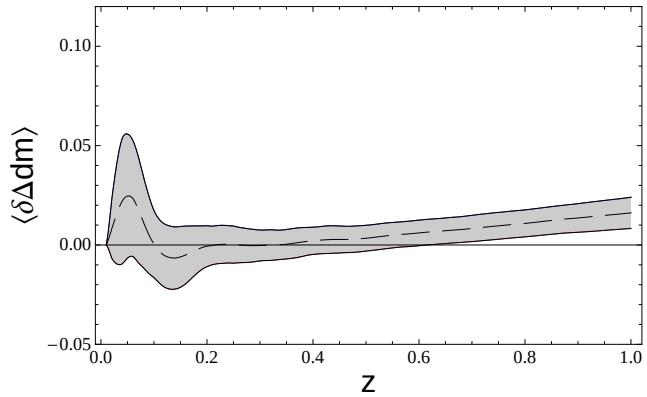

Figure 16. The same as Figure 12, but with a ΛCDM background with $\Omega_\Lambda = 0.7$. This set of voids is from distribution A.

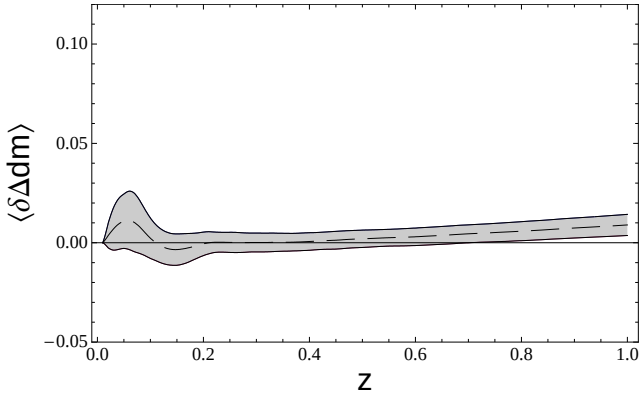

Figure 18. The same as Figure 16, but with the shallow void distribution, B.

lecting observations made over many different lines of sight, at different points on the sky. Such an average is shown in Figure 12. Here 1000 different sets of voids have been generated, their distance moduli calculated, and an average taken. Shown in the plot is the resulting mean deviation from the background value, the central dashed line, and the standard deviation from this value, the shaded region. The effect of w here is to make the location of the edge of the first void random (failing to include w leads to a correlation in the location of the first void, and an increased mean at that point).

The effect of looking at objects in an inhomogeneous universe of this kind is two-fold. Firstly, there is a systematic deviation away from the distance modulus of the background. This appears to be largest at low redshift ($z < 0.1$), when the effect of looking at objects inside voids is considerable, and again at large distances ($z > 0.5$), when the small lensing effect due to looking through voids accumulates. These deviations are moderate for the void distributions chosen here, with $\langle \delta\Delta\mathrm{dm} \rangle < 0.1$, but are clearly non-zero. Such an effect, if unaccounted for, could lead to a systematic bias in extracting cosmological parameters. Secondly, there is a non-zero dispersion around the mean. The effect of having a distribution of voids between us and the source should be expected to result in a typical source being somewhat displaced from the mean. Again, the effect caused by this is largest at small redshifts ($z < 0.2$).

4.1.2 Distribution B: Shallow voids

Having considered one particular distribution of voids, let us now consider a second so that we can better understand the effect of the choice of voids on the resulting averaged distance moduli. From the above considerations of single voids, we know that the maximum displacement of distance modulus is sensitive to the depth of void. We will therefore

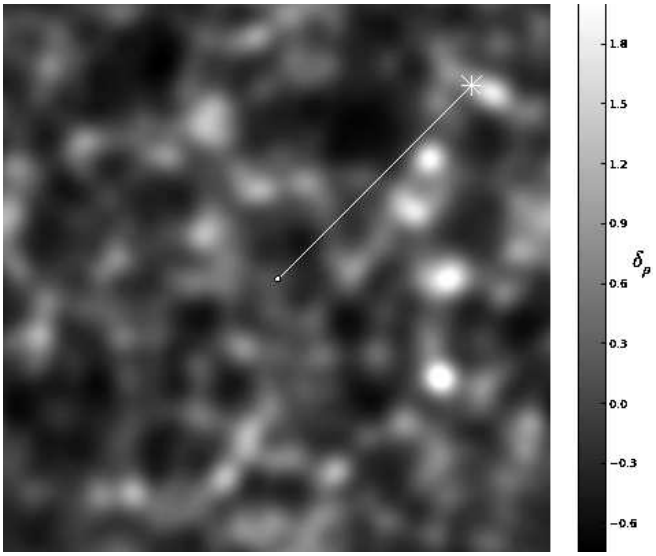

Figure 19. A slice through the Millennium Simulation, smoothed on scales of 10Mpc. The field is 715 Mpc across, the full size of the simulation. An example line of sight to a supernova is shown.

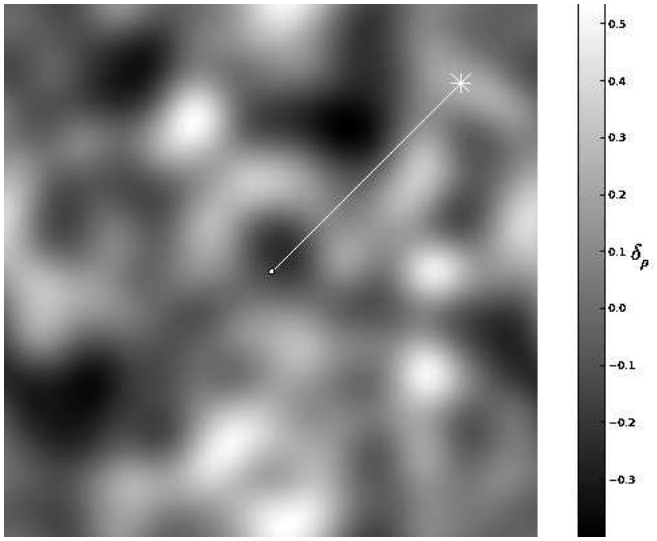

Figure 20. The same Millennium Simulation slice as in Figure 19, but smoothed on 20Mpc scales.

alter the probability distribution from which the void depth is drawn. We will now consider voids from a flat distribution that are between 0% and 50% under-dense at their centre today, with the same distribution of widths as before. A sample density profile and distance modulus plot, for voids drawn from this new distribution, is shown in Figure 13. This can be seen to be similar to the results shown in Figure 11, but with the deviations from the background value reduced.

In order to find the mean, and standard deviation, for this new distribution we will proceed as before. 1000 sets of voids are generated, their distance moduli calculated, and then averaged. The results of this are shown in Figure 14. These results are again similar to those obtained from the previous distribution, except with the magnitude of the deviations from the background model decreasing in a proportionate way to the void depth. The scatter around the mean is similarly decreased.

4.2 A ΛCDM background

Having discussed the situation of looking through many voids in an EdS background, we will also be interested in space-times with a non-zero Λ. In this section we will consider a background ΛCDM cosmology with $\Omega_\Lambda = 0.7$. We will take voids from the same two distributions considered above.

4.2.1 Distribution A: Deep voids

Using the same distribution of deep voids as above (that is with central under-densities between 0% and 75% today), we generate 1000 sets of randomly selected voids. An example set is shown in Figure 15.

In Figure 16 we show the result of averaging over 1000 different sets of randomly generated voids. What is shown here is the deviation from the $\Omega_\Lambda = 0.7$ background value. As before, the central dashed line shows mean deviation, and the shaded region shows the standard deviation from this mean. These results can be seen to be similar to those shown in Figure 12, but with a smaller displacement of the mean, and dispersion around that mean. This is in keeping with the result found in the single void case, that the deviation of the distance modulus, due to the voids, is smaller with non-zero Λ.

4.2.2 Distribution B: Shallow voids

Finally, let us consider $\Omega_\Lambda = 0.7$ with the distribution of shallow voids, where the central under-densities are between 0% and 50%. An example set of voids, out to $z = 1$, is shown in Figure 17. The effect of these shallower voids is similar to the results found above, but with smaller displacements of distance modulus from the background value, as expected.

Figure 18 shows the results of averaging over 1000 sets of voids generated from this distribution. As with the case of deeper voids, the results are similar to those obtained when $\Lambda = 0$, shown in Figure 14, but with smaller displacement of the mean, and dispersion around that mean.

5 SIMULATED STRUCTURE

In sections 3 and 4 we used exact Swiss Cheese cosmologies to determine the effect of large inhomogeneities on luminosity distances. These situations are of interest as they allow unambiguous, explicit calculations to be performed within them. The draw-back of this formalism, however, is that while the theory is non-perturbative, the mass distributions that can be modelled must be highly symmetric. This is in contrast to the linearised approach, where the theory is approximated, but can then be applied more straightforwardly to general mass distributions. Despite these difficulties, we will of course be interested in what the results we have found imply for more realistic situations.

To address the problem of applying this formalism to more realistic mass distributions we will take simulations of what real density fields in the Universe are believed to look like. These density fields will then be idealised so as

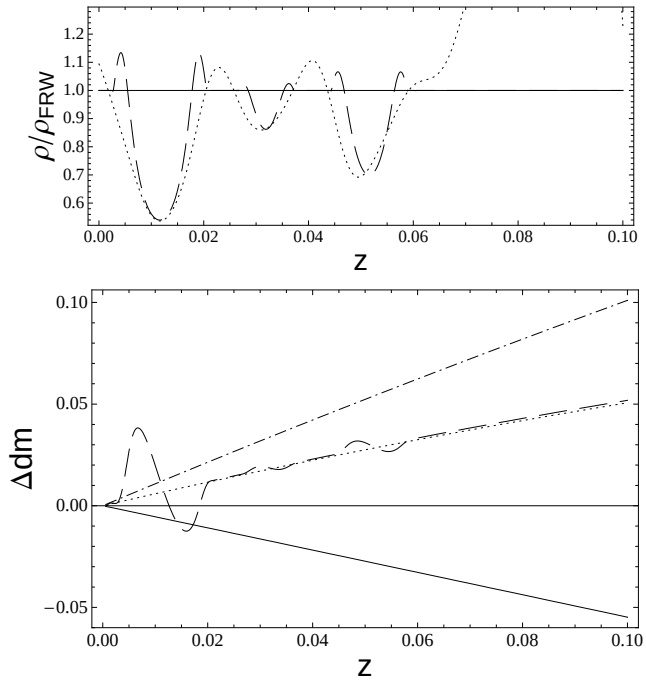

Figure 21. The upper panel shows the density along the line of sight path shown in Figure 19 as the dotted line, and the energy density of our idealised Swiss Cheese as the dashed line. The lower panel shows the distance modulus generated by Swiss Cheese as the dashed line. The smoothing scale here is 10Mpc.

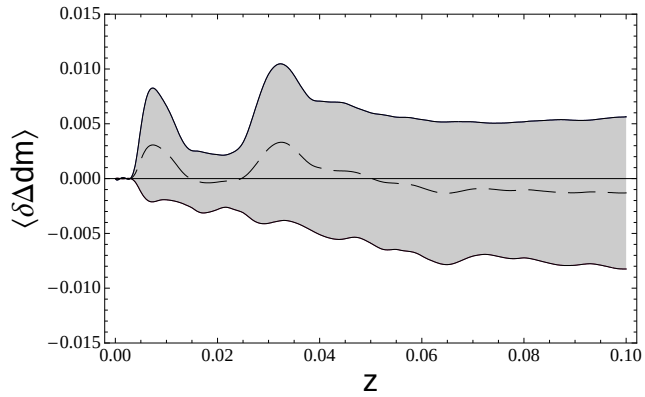

Figure 22. The same as Figure 12, but for the Millennium Simulation smoothed on 10Mpc scales.

to appear as Swiss Cheese: Over-dense regions will be taken as FRW cheese, and under-dense regions will be modelled as LTB holes (with the appropriate width and depth). The real Universe, of course, is not an exact Swiss Cheese, and so our idealisation will require some considerable approximation. In particular, under-densities will not in general be spherically symmetric, but will have different expansion rates in different directions. Our goal here, then, must not be considered a precision calculation of luminosity distances in these simulations, but rather to derive a well motivated distribution of voids that can be used in our Swiss Cheese models (rather than just considering idealised distributions). One would hope that results derived in this way would be more indicative of what may be expected in the real Universe.

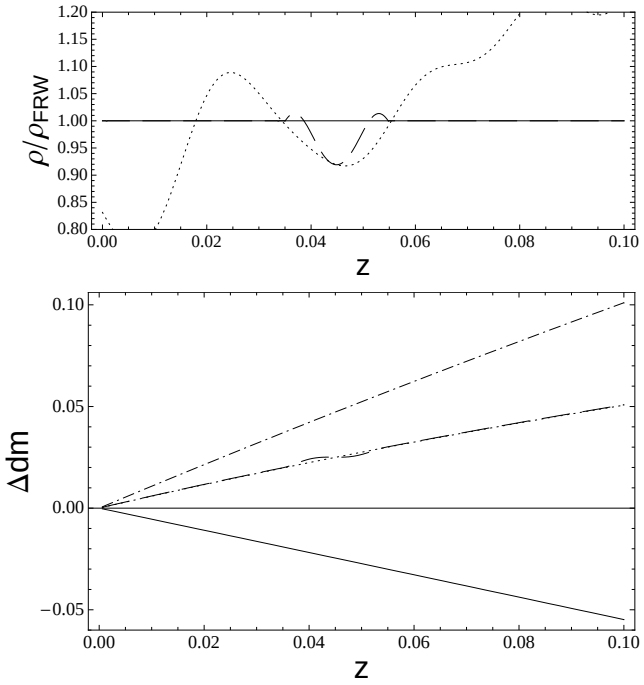

Figure 23. The same line-of-sight density profile, fitted voids, and distance modulus plots as in Figure 21, but for the Millennium Simulation smoothed on 20Mpc scales.

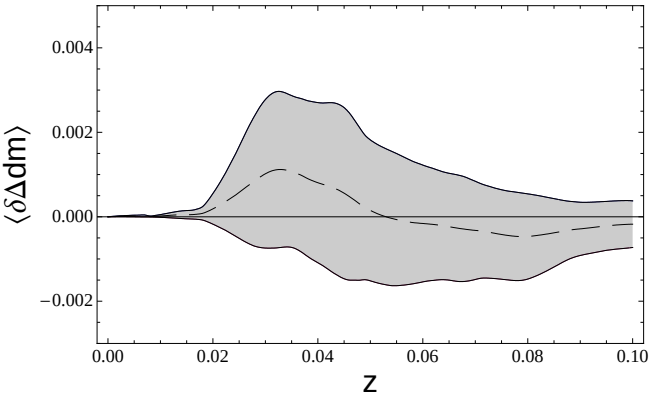

Figure 24. The same as Figure 22, but for the Millennium Simulation smoothed on 20Mpc scales.

5.1 Density Fields

Extracting real density profiles from redshift surveys in the face of limited survey regions, and redshift-space distortions, is somewhat complex (Fisher et al. 1995; Erdogdu 2004). In addition, the formalism we have used up to this point takes density along a space-like projection of a line of sight into a surface of constant t, whereas real observations are made along past light cones. We will therefore use simulations of structure formation to generate line-of-sight profiles of the energy density. These simulations all have $\Omega_\Lambda = 0.7$ in their backgrounds.

While it is the case that the simulations we will be using are derived within the regime of linear perturbations about an FRW background, this does not stop us using these density fields to motivate 'realistic' distributions of voids. The linear nature of the underlying simulations suggests that, in

fact, a linear treatment of luminosity distances and redshifts should be adequate to accurately calculate Hubble diagrams in this space-time. The purpose of this section is not to supersede such studies, but rather to compliment them with a study of Swiss cheese models.

As a simulation of non-linear structure we use the results of the Millennium N-body Simulation (Lemson et al. 2006; Springel 2006). The Millennium Simulation modelled a cubic region of space with a side length of $500/h$ Mpc, where $h \equiv H_0/100 \text{ km s}^{-1}\,\text{Mpc}^{-1} = 0.7$. It modelled 10^{10} dark matter particles in 256^3 cells with periodic boundary conditions, which for our purposes are especially suitable for smoothing on new scales. The database for the simulation[3] directly stores densities smoothed on various scales from 1.25Mpc to 10.0Mpc.

The size of density fluctuations is determined, at least in part, by the smoothing scale applied to the data (the radius of the Gaussian kernel convolved with the data). Our choice of smoothing scale for the non-linear simulation is critical. On small smoothing scales fluctuations are very large, but in these regimes the pressureless dust approximation of the LTB model could break down. In addition, on very small scales discrete particles (i.e. galaxies) may become resolvable, and the fluid approximation itself could then be in question. However, if we choose the smoothing scale to be too large then we will under-estimate the density fluctuations, and hence the effect on the distance modulus. We use smoothing scales of 10 and 20 Mpc; the former is direct from the Millennium database and the latter is manually smoothed with a Gaussian filter. Slices through the smoothed Millennium Simulation are shown in Figures 19 and 20. The former has a smoothing scale of 10Mpc, and the latter is the same density field with a smoothing scale of 20Mpc.

5.2 Distance Moduli

In the density fields under consideration, lines of sight are taken in random directions from the centre of the simulation. We then convert the density profiles along these lines into sets of voids that can be used as input for the formalism developed above. We approximate any under-dense segments of the line as being produced by a void generated from a smooth negative perturbation (33) in the curvature, k, with the same depth and width as the segment. If an under-dense region is split into two by a local maximum that is less than half the depth of its shallowest neighbouring minima, then such an under-density is considered as two voids back to back. Over-dense regions are simply replaced by FRW geometry, with the same density as the background. We also ignore the effect of the local void that, coincidently, happens to lie at the centre of the Millennium Simulation. As mentioned above, local voids have a different effect to the distant voids we are concerned with here.

Let us consider the density fields obtained from smoothing the 10^{10} particles of the Millennium Simulation on different scales. We will begin by considering a smoothing scale of 10Mpc. In this case, the density profile along the example line of sight from Figure 19 is shown in Figure 21. The mean displacement in distance modulus, and standard deviation about that mean, are shown in Figure 22 for a sample of 1000 lines of sight.

As mentioned above, the results we obtain in this section are strongly dependent on the chosen scale of smoothing. Of course, in reality there is only one local expansion rate of space at any given point, but without any knowledge of the smoothing scale to which this corresponds it seems most prudent for us to illustrate the effect of choosing different scales. To this end, we will now consider the results obtained from smoothing on a scale of 20Mpc. In this case the density profile along the example line of sight from Figure 20 is shown in Figure 23, together with the corresponding distance modulus plot.

The mean and standard deviation of the difference in distance modulus from the background value, for 1000 lines of sight, are shown in Figure 24. This plot can be seen to be significantly different to Figure 22: Doubling the smoothing scale has more than halved the magnitude of the displacement and dispersion. Such strong dependence on the smoothing scale shows that understanding the spatial variation of local expansion rates in an inhomogeneous universe could be of critical importance in determining its Hubble diagram.

Studies of luminosity distances in perturbed FRW space-times, such as those of Holz & Wald (1998) and Hui & Greene (2006), find results that appear to be of a similar order of magnitude, although derived in a very different frame-work. For example, Holz & Wald (1998) find that the maximum dimming of the distance modulus from the background value is $\delta\Delta\text{dm}\sim 0.1$ at $z = 0.5$, as well as considerable brightening of some sources due to lensing. The study of Hui & Greene (2006) finds that a displacement of $\delta\Delta\text{dm}\sim 0.1$ could be achieved at larger redshifts, $z \sim 1$, and suggests the interesting possibility of peculiar velocities having a considerable effect on low redshift supernovae, with $z < 0.1$.

6 DISCUSSION

We have considered here the effects of large structures on Hubble diagrams in a non-perturbative way. Using the spherically symmetric LTB exact solution of Einstein's equations we have constructed a Swiss Cheese model of the Universe. In this model the background space-time is taken to be a spatially flat FRW universe, filled with dust and a cosmological constant. Spherically symmetric regions of this background cosmology are then removed and replaced with the regions of negatively curved LTB space-time, matched appropriately at the boundary. The resulting cosmology has an initially evenly distributed energy density. The regions with negative spatial curvature then expand more quickly than the background, and large under-dense voids form. These voids behave like open FRW space-time at their centre and transition smoothly to over-dense regions at their edge, before matching onto the background. Such a universe is an exact inhomogeneous solution of Einstein's equations, with a simple enough geometry to allow calculations of luminosity distances to be performed within it.

By considering the cross-sectional area of a bundle of radial null geodesics, focused on an observer in the back-

[3] http://www.mpa-garching.mpg.de/millennium/

ground space-time, it is possible to obtain a simple analytic expression for the angular diameter distances such an observer will infer for objects in, and beyond, the void. The luminosity distance then follows straightforwardly, and we can calculate the Hubble diagram that our observer will see along such a line of sight. The expressions used are limited to spherically symmetric voids, and to lines of sight that look directly through their centres, but have the great benefit that they are exact. As such, all non-linear effects due to position dependent spatial curvature, expansion rates, and energy densities are automatically included.

We then consider the effect of a single large void on Hubble diagrams constructed by an observer looking through it. We find that observations of objects beyond the void are not noticeably affected by its presence: Deviations from the background value are less than 0.012 magnitudes, for the voids considered. When viewing objects within the void, however, the effect of the voids presence can be of some size. We illustrate the differences witnessed by our observer by considering the distance modulus of astrophysical objects. This is given by the magnitude of a source, minus the magnitude it would have at the same redshift in an empty Milne universe. We consider voids with an even distribution of gravitational mass, and a smooth under-density in spatial curvature. In this case the magnitude to an object in the void is altered by the voids presence. This effect is most pronounced at low redshifts (with $z < 0.2$), while at higher redshifts it drops off, and becomes comparable to the small effect of looking through voids. The maximum displacement from the background distance modulus appears proportionate to the fractional under-density at the centre of the void, and decreases with increasing Λ. This can be seen from Figures 3 and 6, where the relation between void depth and distance modulus displacement can be seen to mildly super-linear. We note that this effect appears to be largely due to $O(0.1)$ perturbations in the metric functionals, and so may be less apparent in a perturbative treatment.

Having studied the case of a single void, we then move on to consider a universe containing many voids. In this case we draw the void widths and depths randomly from probability distributions. We consider a shallow distribution of voids, in which the void depths are between 0% and 50% under-dense at their centre, and and a deeper distribution, in which they are up to 75% under-dense. By generating 1000 sets of voids from each distribution, we produce a mean deviation from the background distance modulus, and the standard deviation that should be expected from that mean. As found in the case of single voids, the displacement of the distance modulus from the background value is proportionate to the depth of voids considered. The dispersion is similarly dependent on typical void depth.

Using data from the Millennium Simulation, we then proceed to consider how structures in more realistic universes could affect the Hubble diagrams constructed by observers in them. To achieve this we take a number of different lines of sight from a central position in the simulation. The density profile along these lines are determined by smoothing on different scales. We then treat under-densities as being formed from spherically symmetric, smooth, negative perturbations in k, and calculate the distance moduli along lines of sight that pass through them. Over-densities are replaced by regions of FRW space-time, with the background density and expansion rate.

The effects of the voids in the Millennium Simulation are small, but non-zero. We find that such voids could have a noticeable effect on the Hubble diagrams constructed by observers in the space-time, by producing deviations and dispersion in the distance modulus. The magnitude of this effect, however, is strongly dependent on the depth of voids, which is itself a function of how the smoothing from discrete sources, to continuous fluid is performed. Increasing the smoothing scale decreases the depth of void, and hence decreases the effect on the Hubble diagram. Ultimately, it appears that one needs to know the appropriate scale on which to smooth, if one wants to make reliable quantitative predictions. We do not attempt to solve this problem here.

We find the non-linear effects of inhomogeneity in the Universe can both displace the average distance modulus from its background value, and introduce dispersion around that average. These effects, if improperly accounted for in fitting data to FRW models, could lead to systematic errors in extracting cosmological parameters, and an underestimation of the errors involved. Such an effect may be of use for accounting for some of the 'intrinsic error' usually added to supernovae data when fitting to cosmological models, and which is often a large fraction of the total error. We find that the the magnitude of these effects is sensitive to the depths of voids involved, their width, and their distance from us.

The study we have performed here is limited in a number of respects, and rather than being exhaustive is instead intended to be a thorough investigation of the simplest case. One will certainly be interested in the effects introduced by different void profiles. It will also be of much interest to determine the effects of looking through voids in an off-centre way. It was suggested by Vanderveld, Flanagan & Wasserman (2008) that such observations can be considerably different to observations directly through the centre. Generalising the present study to off-centre observations is not trivial, but is certainly possible, and we will consider this elsewhere. The studies of Biswas & Notari (2008) and Brouzakis, Tetradis & Tzavara (2007, 2008) suggest that considering off-centre trajectories could have important effects. There are also issues of bias that one may wish to take into account in more detailed studies. For instance, it may be the case that more supernovae occur in denser regions of the Universe, or that supernovae in less dense regions are easier to observe.

This study could be further generalised by considering non-spherical voids, and by better accounting for over-dense regions of the Universe. The LTB voids considered here are only solutions as long as pressure is negligible. A similar study including anything approaching a realistic over-density will therefore require solutions with more general fluid content, which are considerably more difficult to find. It is feasible that the inclusion of over-densities in a more satisfactory way could cancel some of the displacement effect, but it is hard to see how it could counteract the dispersion. In Appendix A we consider the effect of having spherically symmetric shells of under-density, rather than spherical holes (an Onion universe, rather than Swiss Cheese). In this case the effects of the under-densities produce deviations in the distance modulus with the same order

of magnitude, but with the opposite sign, to Swiss Cheese. This shows that a full understanding of the way that large scale structure effects Hubble diagrams is likely to be a complicated function of the detailed geometry of the inhomogeneous Universe. A specialised study of the effect on Hubble diagrams of living in an Onion universe has been performed by Biswas, Mansouri & Notari (2006), and agrees with what we find in Appendix A.

Finally, one may speculate on the effects of large scale structure as potentially mitigating the need for Dark Energy. We find that the voids required to mistake an Einstein-de Sitter background for ΛCDM with $\Omega_\Lambda = 0.7$ would have to be very deep. Even the void distribution considered in Figure 14 does not come close. The voids involved would likely have to be more than 75% under-dense at their centre. Even if such voids did exist, their ability to mimic the shape of the distance modulus of ΛCDM would rely on some fortuitous correlations in their positions, so that the mean Δdm peaks at around $z \sim 0.5$ and drops off at lower redshifts. Alternatively, one may consider extending the present study so that the background Cheese is spatially curved, or so that we are at the centre of a void. The effects of a local void have been shown by a number of authors to be able to mimic, at least to some degree, the presence of Λ on the Hubble diagram (Alexander, Biswas & Notari 2007; Alnes, Amarzguioui & Grøn 2006; Garcia-Bellido & Haugboelle 2008; Clifton, Ferreira & Land 2008; Bolejko & Wyithe 2008), but requires a very deep and wide structure.

ACKNOWLEDGEMENTS

We are grateful to C. Clarkson, P. Ferreira and J. Silk for helpful suggestions and discussion. TC acknowledges the support of Jesus College, and JZ acknowledges that of the STFC. We are also grateful to have received support from the BIPAC, and helpful suggestions from an anonymous referee.

REFERENCES

Alexander S., Biswas T., Notari, A., 2007, arXiv: 0712.0370 [astro-ph].
Alnes H., Amarzguioui M., Grøn Ø., 2006, PRD, 73, 083519.
Biswas T., Mansouri R., Notari A., 2007, JCAP, 0712, 017.
Biswas T., Notari A., 2008, JCAP 0806, 021.
Bolejko K., Wyithe J. S. B., 2008, arXiv:0807.2891 [astro-ph].
Bondi H., 1947, MNRAS, 107, 410.
Bonnor W. B., 1974, MNRAS, 167, 55.
Bonnor W. B., Vickers P. A., 1981, Gen. Rel. Grav., 13, 29.
Bonvin C., Durrer R., Alice Gasparini M., 2006, PRD, 73, 023523.
Brouzakis N., Tetradis N., Tzavara E., 2007, JCAP, 0702, 013.
Brouzakis N., Tetradis N., Tzavara E., 2008, JCAP, 0804, 008.
Clifton T., Ferreira P. G., Land K., 2008, PRL, 101, 131302.
Dyer C. C., Roeder, R. C., 1972, ApJ, 174, L115.
Dyer C. C., Roeder R. C., 1973, ApJ, 180, L31.
Dyer C. C., Roeder R. C., 1974, ApJ 189, 167.
Ellis G. F. R., Nel S. D., Maartens R., Stoeger W. R. & Whitman A. P., 1985, Phys. Rep. 124, 315.
Erdogdu P. et al., 2004, MNRAS, 352, 939.
Etherington I. M. H., 1933, Phil. Mag., 15, 761.
Fisher K. et al., 1995, MNRAS, 272, 885.
Frieman J. A., 1996, astro-ph/9608068.
Futamase T., Sasaki M., 1989, PRD, 40, 2502.
Garcia-Bellido J., Haugboelle T., 2008, JCAP, 04, 003.
Granett B. R., Neybrinck M. C., Szapudi I., 2008, ApJ, 683, L99.
Hogg D. W. et al., 2005, ApJ, 624, 54.
Holz D. E., Wald R. M., 1998, PRD, 58, 063501.
Hui L., Greene P. B., 2006, Phys. Rev., D73, 123526.
Inoue K. T., Silk J., 2006, ApJ, 648, 23.
Kantowski R., 1998, ApJ, 507, 483.
Kasai M., Futamase T., Takahara F., 1990, Phys. Lett. A, 147, 97.
Land K., Magueijo J., 2005, PRL, 95, 071301.
Lemaître G., 1933, Ann. Soc. Sci. Brussels, A53, 51.
Lemson G. and the Virgo Consortium, 2006, astro-ph/0608019.
Lewis A. et al., 2000, ApJ, 538, 473.
Marra V. et al., 2007, PRD, 76, 123004.
Mattsson T., 2007, arXiv:0711.4264 [astro-ph].
Pyne T., Birkinshaw M., 2004, MNRAS, 348, 581.
Ribeiro M. B., 1992, ApJ, 388, 1.
Sachs R., 1961, Proc. Roy. Soc. A, 264, 309.
Sasaki M., 1987, MNRAS, 228, 653.
Springel V. et al., 2005, Nature, 435, 629.
Sugiura N., Sugiyama N., Sasaki M., 1999, Prog. Theo. Phys., 101, 903.
Sylos Labini F. et al., 2008, arXiv:0805.1132 [astro-ph].
Sylos Labini F. et al., 2009a, Europhys. Lett., 85, 29002.
Sylos Labini F. et al., 2009b, A & A, 496, 7.
Tolman R. C., 1934, Proc. Nat. Acad. Sci. USA, 20, 169.
Vanderveld R. A., Flanagan E. E., Wasserman I., 2008, PRD, 78, 083511.
Watkins R., Feldman H. A., Hudson M. J., 2008, arXiv:0809.4041 [astro-ph].
Zecca A., 1991, Nouvo Cim., B106, 413.

APPENDIX A: AN ONION UNIVERSE

As an alternative to considering the Swiss Cheese model, one can also use the LTB solution to consider an 'Onion Universe', in which there are under-dense shells of matter in a spherically symmetric space-time. Although less appealing as a way of modelling the real inhomogeneous Universe, a brief consideration of luminosity distances in such a space-time will allow us to put the Swiss Cheese results in some context. An example of the spatial curvature profile of an Onion universe is given in Figure A1, where a surface of constant time is shown, with one spatial dimension suppressed. Vertical displacement indicates a fluctuation in k, and distance from the centre is proportional to comoving distance, r.

The observer in this space-time is taken to be at the centre of symmetry, so that the luminosity distance to a

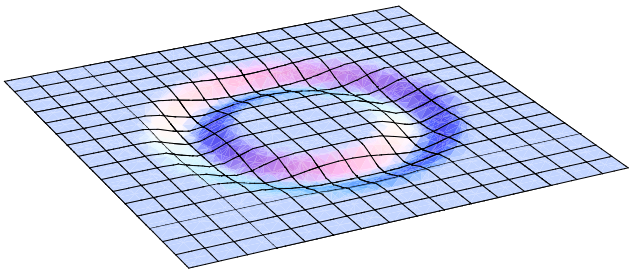

Figure A1. An illustration of $k(\mathbf{x})$ in an Onion universe. The surface displayed is a constant time slice, with one spatial dimension suppressed. Vertical displacement indicates a fluctuation in k, and distance from the centre is proportional to the coordinate distance, r.

source at (t_e, r_e) is given by (32). In Figure A2 we show a couple of example cases. The radial profile of the curvature perturbation in each of these cases is that of (33), with its minimum displaced from the centre of symmetry. The upper panel in Figure A2 shows the energy density, as a function of redshift, experienced by the photon as it travels along our past light cone. While the perturbation in $k(r)$ is symmetric, the resulting energy density distribution can be seen to be highly asymmetric, with a considerable over-density on the side of the under-dense shell that is furthest from the observer.

In the lower panel of Figure A2 we plot the distance modulus that would be measured by an observer at the centre of symmetry, for these two different cases. It can be seen that the under-density produces a considerable deviation from the background EdS model. Comparing this effect with that shown in Figure 1, for the Swiss Cheese case, one can see that the magnitude of the deviation is of the same order. More striking, however, is that the under-density in the Onion universe causes a very different deviation in distance modulus.

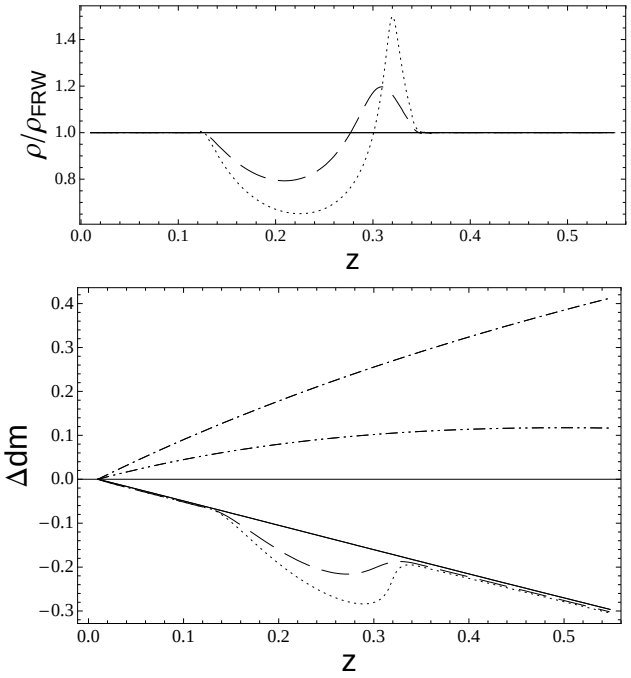

Figure A2. The upper panel shows two example density profiles resulting from smooth perturbations in $k(r)$ of the form (33), with different depths. The lower panel shows the corresponding distance moduli. The dot-dashed, double-dot-dashed and solid lines are as in Figure 1.